THE JOURNAL OF BIOLOGICAL CHEMISTRY VOL. 281, NO. 43, pp. 32784–32795, October 27, 2006

Structural Basis for Inhibition of Protein-tyrosine Phosphatase 1B by Isothiazolidinone Heterocyclic Phosphonate Mimetics*

Received for publication, July 19, 2006, and in revised form, August 14, 2006 Published, JBC Papers in Press, August 17, 2006, DOI 10.1074/jbc.M606873200

Paul J. Ala[1], Lucie Gonneville, Milton C. Hillman, Mary Becker-Pasha, Min Wei, Brian G. Reid, Ronald Klabe, Eddy W. Yue, Brian Wayland, Brent Douty, Padmaja Polam, Zelda Wasserman, Michael Bower, Andrew P. Combs, Timothy C. Burn, Gregory F. Hollis, and Richard Wynn

From the Incyte Corp., Wilmington, Delaware 19880

Crystal structures of protein-tyrosine phosphatase 1B in complex with compounds bearing a novel isothiazolidinone (IZD) heterocyclic phosphonate mimetic reveal that the heterocycle is highly complementary to the catalytic pocket of the protein. The heterocycle participates in an extensive network of hydrogen bonds with the backbone of the phosphate-binding loop, Phe^{182} of the flap, and the side chain of Arg^{221}. When substituted with a phenol, the small inhibitor induces the closed conformation of the protein and displaces all waters in the catalytic pocket. Saturated IZD-containing peptides are more potent inhibitors than unsaturated analogs because the IZD heterocycle and phenyl ring directly attached to it bind in a nearly orthogonal orientation with respect to each other, a conformation that is close to the energy minimum of the saturated IZD-phenyl moiety. These results explain why the heterocycle is a potent phosphonate mimetic and an ideal starting point for designing small nonpeptidic inhibitors.

Protein-tyrosine phosphatase 1B (PTP1B)[2] is considered to be one of the best validated drug targets for the treatment of type II diabetes. The enzyme is localized to the cytoplasmic face of the endoplasmic reticulum where it negatively regulates insulin signaling by dephosphorylating phosphotyrosine (Tyr(P)) residues in the kinase regulatory domain of the insulin receptor (IR) (1, 2). Mice lacking the homolog of PTP1B have lower blood glucose levels and improved insulin responsiveness compared with normal and diabetic mice through enhanced IR signaling in peripheral tissues (3, 4). Similar results were also observed when an antisense oligonucleotide was injected into mice (5). These compelling biological results coupled with the wealth of structural data, which have been generated since the crystal structure of PTP1B was determined in 1994 (6), have contributed to the rapid design of many potent inhibitors (7–13). Unfortunately, poor physicochemical properties have limited their development as drug candidates.

Crystal structures of PTP1B in complex with phosphorylated peptides corresponding to the IR kinase activation segment (14) and an autophosphorylated site of the epidermal growth factor receptor (15) reveal that the highly negatively charged substrates bind to multiple positively charged sites (Fig. 1*a*). The catalytic site, which is located at the base of a shallow pocket called the primary phosphate-binding pocket or A site, is the most polar region of the protein, and it contains the phosphate-binding signature motif (Cys^{215}–Arg^{221}) common to all members of the protein-tyrosine phosphatase family (16). A second phosphate-binding pocket (B site), adjacent to the A site, was identified from the crystal structures of the protein in complex with a small aryl phosphonate (17) and a bisphosphorylated peptide (14). The B site, which is larger and shallower than the A site and has lower binding affinity for aryl phosphates, is noncatalytic but may play an important role in determining substrate specificity. A third phosphate-binding site (C site) was identified when the distal Tyr(P) mimetic of a bisphosphonate-containing inhibitor unexpectedly bound in a large flat region of the protein near Lys^{41} and Arg^{47} (18). Overall, the active site of PTP1B possesses very few desirable drug-design features. The highly charged A site and flat, solvent-exposed B and C sites significantly increase the difficulty of designing potent inhibitors with acceptable membrane permeability. In the past 10 years, many anions that mimic the interactions of phosphate, in the A site, have been incorporated into the design process (19). The most potent include the following: oxalylaminothiophene carboxylic acid (OTCA), carboxymethoxybenzoic acid (CMBA), oxalylaminobenzoic acid, and difluoromethylphosphonic acid (DFMP) (Fig. 1*b*). Unfortunately, the resulting compounds have poor membrane permeability because their highly charged phosphonate mimetics are ionized at physiological pH.

We have recently reported the design of a novel five-membered isothiazolidinone (IZD) heterocyclic phosphonate mimetic that possesses only a single delocalized negative charge (Fig. 1*b*) (20). IZD-containing compounds are potent competitive inhibitors of PTP1B, but more importantly, they have been

* The costs of publication of this article were defrayed in part by the payment of page charges. This article must therefore be hereby marked "*advertisement*" in accordance with 18 U.S.C. Section 1734 solely to indicate this fact.

The atomic coordinates and structure factors (code 2CM2, 2CM3, 2CM7, 2CM8, 2CMA, 2CMB, and 2CMC) have been deposited in the Protein Data Bank, Research Collaboratory for Structural Bioinformatics, Rutgers University, New Brunswick, NJ (http://www.rcsb.org/).

[1] To whom correspondence should be addressed: Incyte Corp., Experimental Station, Rte. 141 and Henry Clay Rd., Wilmington, DE 19880. E-mail: pauljala@gmail.com.

[2] The abbreviations used are: PTP1B, protein-tyrosine phosphatase 1B; Tyr(P), phosphotyrosine; IR, insulin receptor; OTCA, 2-(oxalyl-amino)-thiophene-3-carboxylic acid; CMBA, 2-carboxymethoxybenzoic acid; DFMP, difluoromethylphosphonic acid; IZD, isothiazolidinone; TCEP, tris(2-carboxyethyl)phosphine hydrochloride; PDB, Protein Data Bank; r.m.s.d., root mean square deviation.

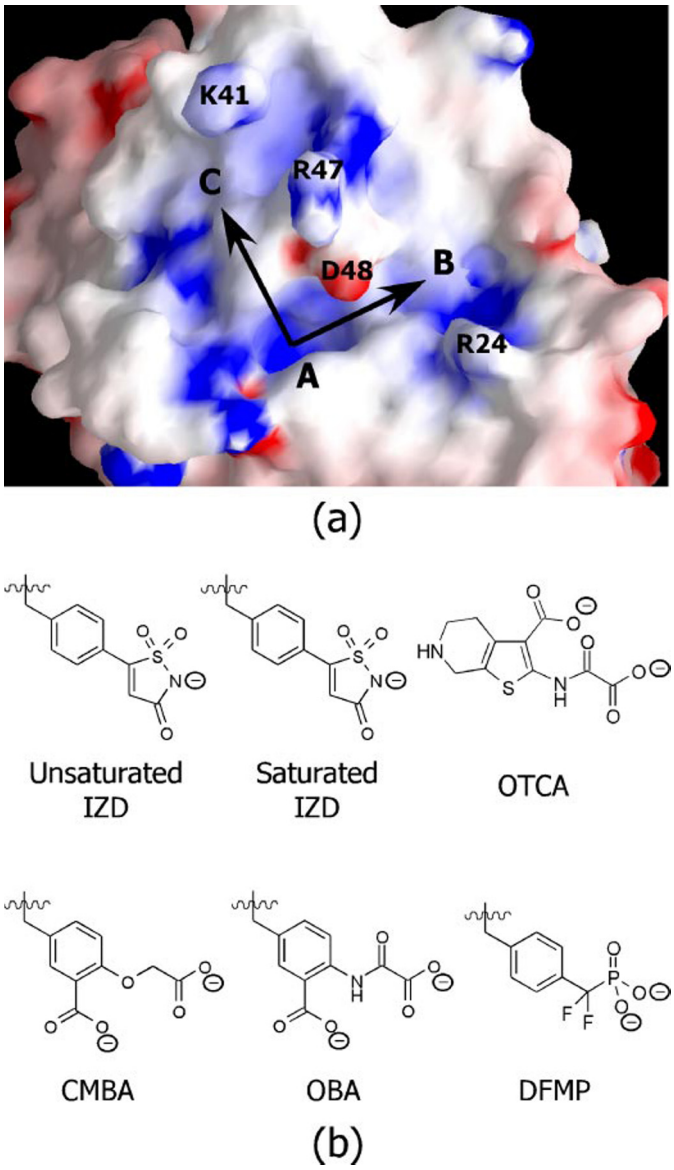

FIGURE 1. *a,* surface potential of the PTP1B active site. The positively charged A site (primary phosphate-binding pocket) is the most polar region of the protein and contains the catalytic site where phosphate ions interact with the signature motif; B site is the secondary phosphate-binding pocket that plays a role in substrate specificity; C site is a large flat region that can accommodate negatively charged substituents. *Arrows* indicate that most reported inhibitors bind in the A site and extend into the B and/or C sites; all inhibitors reported in this study bind in the A and C sites. *b,* known phosphotyrosine mimetics shown in ionized form expected at physiological pH; note the saturated and unsaturated IZD heterocycles possess a single negative charge. *OBA*, oxalylaminobenzoic acid.

shown recently to have cellular activity in an IR phosphorylation assay (21). The IZD ring was specifically designed to incorporate all previously observed binding features of known phosphonate mimetics. For example, it simultaneously mimics the interactions of the three phosphate oxygens of DFMP, which is arguably the most potent phosphonate mimetic, and the carboxymethyl group of CMBA (Fig. 2*a*). Combining these features into a single heterocycle has produced one of the most potent phosphonate mimetics reported to date. One of our most potent IZD-containing peptides (compound **8**) has an IC_{50} value of 190 nM, which is ~9-fold more potent than the equivalent DFMP-containing analog (Table 3). In order to gain insights into the structural basis for inhibition of PTP1B by IZD-containing compounds, we have solved the crystal structures of the protein in complex with IZD-phenol and several IZD-containing peptides (Table 2). Identifying the key binding interactions should aid the design of small molecule inhibitors as well as the design of even more potent, less polar phosphate mimetics.

EXPERIMENTAL PROCEDURES

Protein Expression

Two constructs of the catalytic domain of human PTP1B (435 amino acids), 1–321 and PTP1B-(1-His_6-298), were expressed in *Escherichia coli* essentially as described previously (22). Briefly, BL21(DE3)-competent cells (Novagen) were transformed with the expression plasmids as described by the manufacturer. LB broth (2 ml) containing 100 μg/ml ampicillin was inoculated with a single colony from an ampicillin-containing LB agar plate and incubated in a 15-ml tube for 2 h of shaking at 225 rpm at 37 °C. The culture was then used to inoculate 50 ml of Terrific Broth (Media Tech) containing 100 μg/ml ampicillin in a 500-ml vented Erlenmeyer flask. The following day, the 50-ml culture was used to inoculate 1 liter of Terrific Broth/ampicillin in a 3-liter vented Fernbach culture flask. When the A_{600} reached 1, 0.5 mM isopropyl β-D-thiogalactopyranoside was added, and the culture was incubated for 16 h of shaking at 75 rpm at 27 °C. The culture was pelleted at 5,800 × *g*, immediately frozen on dry ice, and stored at −80 °C.

Protein Purification

Cell paste was suspended (5 ml/g of cells) at 4 °C in buffer A (20 mM Tris, pH 7.5, 150 mM NaCl, 10% glycerol, 100 μM leupeptin, 1 μM pepstatin A, and 1 mM phenylmethylsulfonyl fluoride (Sigma)) and stirred for 15 min. The mixture was then homogenized for 30 s using an Ultra-Turrax T 25 basic (IKA Works, Inc.), lysed using an EmulsiFlex-C5 homogenizer (Avestin, Inc.) with two passes at 10,000–15,000 p.s.i., and then centrifuged at 11,000 × *g* for 30 min. The supernatant containing soluble PTP1B-(1-His_6-298) was mixed with Talon metal affinity resin (BD Biosciences) at a protein to resin ratio of 10:1 (mg/ml) and stirred for 2 h. The protein/resin mixture was then poured into a column and washed with buffer A until the eluate $A_{280} < 0.1$. The resin was then washed with 2 column volumes of buffer A containing 10 mM imidazole, and the protein was eluted with buffer A containing 100 mM imidazole.

The supernatant containing soluble PTP1B-(1–321) was mixed with Q-Sepharose Fast Flow resin (GE Healthcare) and placed in a spinner flask overnight at 4 °C. The protein/resin mixture was then filtered through a sintered glass filter, resuspended in buffer B (20 mM Tris, pH 7.5, and 1 mM EDTA), poured into a column, and washed until $A_{280} < 0.1$. The protein was eluted with a linear gradient of NaCl (0–500 mM) in buffer B using a total of 10 column volumes. Column fractions were analyzed by SDS-PAGE, and those containing PTP1B were pooled and mixed with diammonium sulfate (4 M stock) to a final concentration of 1.7 M. The mixture was then diluted with an equal volume of buffer B containing 1.7 M diammonium sulfate and loaded onto a fast flow phenyl-Sepharose column

TABLE 1
Data collection and refinement statistics for apoPTP1B

Protein construct	PTP1B 1-(His_6)-298			PTP1B 1–321
Data collection statistics				
Temperature (°C)	−180	4	−180	−180
Space group	$P2_12_12_1$	$P2_12_12_1$	C2	$P3_121$
Unit cell (Å, °)	$a = 40.6$	$a = 41.1$	$a = 106.8$	$a = b = 88.3$
	$b = 69.2$	$b = 70.4$	$b = 95.5$	$c = 104.1$
	$c = 100.8$	$c = 102.4$	$c = 70.7$	
			$\beta = 109.7$	
Resolution range (Å)[a]	33-1.5 (1.55-1.5)	19-2.0 (2.07-2.0)	27-2.1 (2.18-2.1)	44-2.1 (2.18-2.1)
Molecules/absorbance unit	1	1	2	1
No. of unique reflections	44,327	18,003	38,991	27,186
Average redundancy	4.0 (2.3)	2.5 (2.4)	3.7 (3.7)	5.0 (5.0)
Completeness (%)	95.7 (73.0)	86.9 (89.6)	99.8 (100)	97.4 (95.3)
$\langle I/\sigma \rangle$[b]	16.5 (3.0)	5.1 (1.8)	14.8 (5.6)	17.6 (4.6)
R_{merge} (%)[c]	4.9 (32.4)	10.3 (41.1)	5.8 (13.7)	5.2 (31.0)
Refinement statistics				
No. of protein atoms	2341	2272	4474	2410
No. of solvent atoms	341	127	507	207
No. of heteroatoms	16	0	2	7
Rmsd, bond (Å/°)	0.011/1.54	0.008/1.40	0.008/1.4	0.011/1.54
Resolution range (Å)	33-1.5	19-2.0	27-2.1	44-2.1
R_{factor}/R_{free} (%)[d]	20.1/23.7	21.8/27.7	23.9/29.8	22.8/27.3
Resolution in final structure	[2xHis]-282	3-280	7-280	3-297
PDB ID	2CM2	NA[e]	2CM3	NA

[a] Values in parentheses are for the highest resolution bin.
[b] Average of the diffraction intensities divided by their standard deviations.
[c] $R_{merge} = \Sigma_{hkl}\Sigma_i|I_{hkl,i} - \langle I_{hkl}\rangle|/\Sigma_{hkl}\Sigma_i(I_{hkl,i})$, where $\langle I_{hkl}\rangle$ is the average intensity of the multiple $I_{hkl,i}$ observations.
[d] $R_{factor} = \Sigma_{hkl}||F_o| - |F_c||/\Sigma_{hkl}|F_o|$, where F_o and F_c are observed and calculated structure factor amplitudes for reflection *hkl*, respectively. R_{free} is the same as R_{factor} for a random 10% of reflections excluded from refinement.
[e] NA indicates not applicable.

(GE Healthcare). The protein was eluted with a decreasing diammonium sulfate gradient (1.7–0 M) using 8 column volumes.

Column fractions from both preparations were analyzed by SDS-PAGE, and those containing PTP1B were concentrated to 5 mg/ml using a stirred cell with a YM-10 membrane (Millipore). The concentrated protein (2-ml aliquots) was injected onto a HiLoad Superdex 75 26/60 Prep Grade column connected to an ÁKTApurifier chromatography system (Amersham Biosciences). The column was pre-equilibrated with buffer C (10 mM Tris, pH 7.5, 25 mM NaCl, and 1 mM EDTA) and run at a flow rate of 2.5 ml/min. Fractions containing pure protein were concentrated to 10 mg/ml and stored in 200-μl aliquots at −20 °C. Approximately 20 mg of pure PTP1B was obtained from 12 g of cells.

Biochemical Assay

PTP1B enzymatic assays were performed essentially as described previously (23). Briefly, protein activity was determined by measuring the rate of hydrolysis of *p*-nitrophenyl phosphate. The reaction was performed at room temperature in 25 mM Tris-bis-propane, pH 7.0, containing 5 nM PTP1B, 0.1 mg/ml bovine serum albumin, and 1 mM *p*-nitrophenyl phosphate, which is its K_m value. IC_{50} values were determined by fitting the initial rates of *p*-nitrophenol production to a sigmoidal dose-response equation using Prism 3.0 (GraphPad Software).

Crystallization

The two protein constructs, PTP1B-(1–321) and PTP1B-(1-His_6-298), were crystallized in the presence and absence of inhibitors (dissolved in water pH 7.0). All crystals were grown using the vapor diffusion method with or without microseeding in 24- or 96-well plates in which the protein drops were equilibrated against 1 or 0.15 ml of well solution, respectively, at 4 or 10 °C.

Crystals of PTP1B-(1–321)—The apoprotein crystallized in the trigonal space group $P3_121$ as hexagonal rods (0.3 × 0.2 × 0.01 mm) 7 days after mixing 2 μl of protein (10 mg/ml) with 2 μl of well solution (100 mM Hepes, pH 6.6, 14–16% PEG 8000, and 200 mM magnesium acetate) at 4 °C. Crystals of PTP1B in complex with compounds **1**, **2**, and **3** were grown by mixing 2 μl of protein/inhibitor solution (10 mg/ml protein with 3, 10, and 2.4 mM inhibitor, respectively) with 2 μl of well solution (100 mM Hepes, pH 6.6, 14–16% PEG 8000, and 200 mM magnesium acetate). Hexagonal rods containing compounds **1** (0.06 × 0.06 × 0.12 mm), **2** (0.02 × 0.02 × 0.25 mm), and **3** (0.02 × 0.02 × 0.25 mm) appeared 7–10 days after macroseeding at 4 °C.

Crystals of PTP1B 1-[His_6]-298—The apoprotein crystallized in the orthorhombic $P2_12_12_1$ and monoclinic C2 space groups. The orthorhombic crystals grew into thin plates (0.3 × 0.2 × 0.01 mm) 7 days after mixing 1 μl of protein solution (10 mg/ml protein, 0.025% β-octyl glucoside, and 2 mM TCEP) with 1 μl of well solution (100 mM sodium/potassium phosphate, pH 5.9, and 25–35% methylpentanediol) at 4 °C. The monoclinic crystals grew into large bipyramids (0.2 mm in length) 3–5 days after mixing 2 μl of protein (10 mg/ml) with 2 μl of well solution (12–16% PEG 3000, 100 mM Hepes, pH 7.0–8.0, 200 mM magnesium acetate, and 2 mM TCEP) and microseeding at 4 °C. Rod-shaped crystals of PTP1B/**4** (0.04 × 0.04 × 0.25 mm) appeared 7–10 days after mixing 4 μl of protein/inhibitor solution (10 mg/ml protein, 0.025% β-octyl glucoside, 2 mM TCEP, and 2 mM compound) with 4 μl of well solution (100 mM Hepes, pH 8.5, and 1.12 M sodium citrate) and microseeding at 10 °C. Rod-shaped crystals of PTP1B/**5**

TABLE 2
Data collection and refinement statistics for PTP1B in complex with phosphonate mimetics

	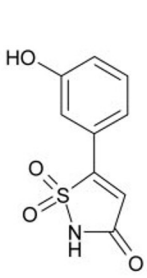	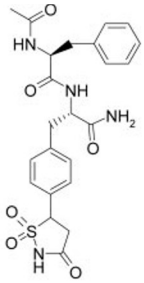	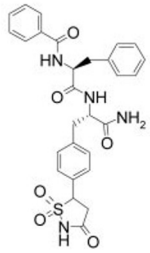	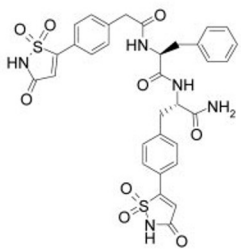	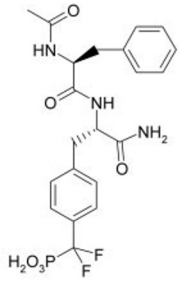
compound					
class	IZD	IZD	IZD	IZD	DFMP
ID	**1**	**2**	**3**	**4**	**5**
IC_{50} (nM)[a]	1350	210	185	65	1750
protein construct	PTP1B 1-321			PTP1B 1-[6xHis]-298	
data collection statistics					
temperature (°C)	-180	-180	-180	-180	-180
space group	$P3_121$	$P2_1$	$P2_1$	$P2_12_12_1$	$P2_12_12_1$
unit cell (Å, °)	a=b= 88.3 c = 104.2	a = 43.9 b = 88.4 c = 49.8 β = 96.8	a = 43.7 b = 88.2 c = 49.8 β = 96.8	a = 60.9 b = 71.2 c = 83.8	a = 62.2 b = 70.9 c = 83.3
resolution range (Å)[b]	32-2.0 (2.14-2.0)	35-2.1 (2.18-2.1)	17-2.3 (2.28-2.2)	31-1.7 (1.8-1.7)	21-2.2 (2.28-2.2)
molecules/au	1	1	1	1	1
no. unique reflections	31292	22079	17624	39170	18789
ave. redundancy	10.6 (10.5)	3.7 (3.7)	2.6 (2.5)	6.9 (6.7)	3.4 (3.3)
completeness (%)	99.6 (98.9)	100 (100)	92.5 (64.6)	100 (100)	97.5 (99.8)
$<I/\sigma>$[c]	32.5(9.4)	11.5 (3.6)	7.3 (2.5)	13.6 (4.0)	9.5 (3.5)
R_{merge} (%)[d]	3.6 (20.5)	6.7 (30.0)	10.4 (37.8)	6.7 (41.1)	8.4 (32.4)
refinement statistics					
no. protein atoms	2433	2418	2418	2356	2341
no. solvent atoms	222	227	192	268	178
no. heteroatoms	22	34	39	68	58
rmsd, bond (Å/°)	0.010/1.51	0.010/1.56	0.008/1.44	0.007/1.35	0.010/1.53
resolution range (Å)	32-2.1	35-2.1	17-2.3	31-1.7	21-2.2
R_{factor} /R_{free} (%)[e]	21.8/25.7	20.4/25.8	20.6/27.8	20.2/22.0	21.5/27.4
res. in final structure	2-298	3-298	3-298	1-[6xHis]-280	[6xHis]-280
PDB ID	2CM8	2CM7	2CMA	2CMB	2CMC

[a] All inhibitors are competitive.
[b] Values in parentheses are for the highest resolution bin.
[c] Average of the diffraction intensities divided by their standard deviations.
[d] $R_{merge} = \Sigma_{hkl}\Sigma_i|I_{hkl,i} - \langle I_{hkl}\rangle|/\Sigma_{hkl}\Sigma_i(I_{hkl,i})$, where $\langle I_{hkl}\rangle$ is the average intensity of the multiple $I_{hkl,i}$ observations.
[e] $R_{factor} = \Sigma_{hkl}||F_o| - |F_c||/\Sigma_{hkl}|F_o|$, where F_o and F_c are observed and calculated structure factor amplitudes for reflection *hkl*, respectively. R_{free} is the same as R_{factor} for a random 10% of reflections excluded from refinement.

(0.05 × 0.05 × 0.3 mm) appeared 10 days after mixing 2 μl of protein/inhibitor solution (10 mg/ml protein, 0.025% β-octyl glucoside, 2 mM TCEP, and 2.4 mM compound) with 2 μl of well solution (100 mM Tris, pH 8.5, and 1.4–1.8 M ammonium sulfate) at 4 °C.

Data Collection

Crystals were transferred stepwise at 1-min intervals into cryoprotectant solutions of mother liquor containing 10 and 20% glycerol and then flash-cooled in a nitrogen stream at −180 °C. For PTP1B/**1** crystals, additional compound (10 mM)

was added to the cryoprotectant solution to prevent the inhibitor from soaking out during the procedure. The orthorhombic apocrystals were cooled in mother liquor without additional cryoprotectant. Diffraction data were collected with one crystal per data set on a Rigaku/MSC RAXIS IV++ imaging system mounted on a Rigaku/MSC MicroMax™-007 rotating anode microfocus generator (CuK_α) operating at 40 kV and 20 mA and equipped with a 0.3-mm cathode, 0.5- and 0.03-mm double collimator, and a Blue Confocal Max-Flux® optical system. Diffraction intensities were integrated and scaled using CrystalClear (Rigaku/MSC).

Structure Determination and Refinement

The orthorhombic and monoclinic apostructures and the structures containing **2** and **4** were solved by molecular replacement using the protein coordinates from the Protein Data Bank (PDB) (24) entry code 1EE0 as the search model and the program CNX (Accelrys). All rotation and translation searches yielded single consistent solutions for data between 15 and 4 Å. The resulting models were subjected to rigid body refinement followed by simulated annealing (using torsion angle dynamics) and positional and temperature factor refinements using CNX. All other structures were solved by difference Fourier methods using the relevant starting model. The conformations of the bound inhibitors were unambiguously determined after one or two cycles of refinement. The final models were generated after several cycles of model building and refinement using QUANTA (Accelrys) and CNX, respectively. Only the (*S*)-IZD stereoisomers of **2** and **3** were observed in the crystal structures even though diastereoisomeric mixtures were used in crystallization experiments. Solvent molecules were added by visual inspection of electron density maps using X-SOLVATE (Accelrys). The final models are consistent with simulated annealed omit maps: **1** (Fig. 2*b*), apo $P2_12_12_1$ (Fig. 3*a*), **4** (Fig. 7*a*), and **2** (Fig. 8*b*). Crystallographic data and refinement statistics are listed in Tables 1 and 2.

RESULTS

To identify the unique structural features responsible for the high potency of IZD-containing compounds, we have determined the crystal structure of PTP1B in complex with the small unsaturated IZD-phenol **1**, which is a potent inhibitor for its size (IC_{50} = 1.35 μM) (Table 2). Crystal structures of PTP1B in complex with unsaturated and saturated IZD- and DFMP-containing peptides were also determined (Table 2) to explain why the saturated IZD **8** is 9- and 16-fold more potent than the equivalent DFMP **5** and unsaturated **6** analogs (Table 3), respectively, as well as identify key interactions outside of the A site that might aid the design of nonpeptidic inhibitors.

IZD Is Highly Complementary to the Primary Phosphate Binding Pocket—The structure of PTP1B/**1** reveals extensive interactions between the inhibitor and the A site. The heterocycle binds at the center of the phosphate-binding loop (Cys^{215}–Arg^{221}), where its four hydrogen bonding acceptors are in the vicinity (2.7–3.3 Å) of 10 donors (Fig. 2*c*). The sulfone oxygens hydrogen bond to N-η of Arg^{221} and the backbone nitrogens of Ser^{216}, Ala^{217}, Gly^{218}, Ile^{219}, and Gly^{220}. The nitrogen anion interacts with the helix dipole of α4 (Arg^{221}–Arg^{238}) and hydrogen bonds to N-ϵ and backbone NH of Arg^{221}, and the carbonyl oxygen hydrogen bonds to the backbone nitrogen of Phe^{182} and side chain of Gln^{266}. An additional hydrogen bond is observed between the side chain of Asp^{181} and the π electrons of the unsaturated IZD. The hydrophobic side of the heterocycle and phenyl ring directly attached to it interact with the hydrophobic half of the A site as follows: Tyr^{46}, Val^{49}, Ala^{217}, Ile^{219}, Phe^{182}, and the aliphatic portion of the side chain of Gln^{262}. The latter van der Waals interactions and the extensive network of hydrogen bonds are key reasons why IZD-phenol is a potent inhibitor.

IZD Displaces All Tightly Bound Waters in the A Site—The recently reported high resolution crystal structure of the

TABLE 3
Phosphonate mimetic SAR

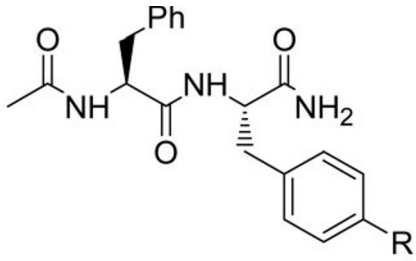

Cmpd	Phosphonate Mimetic	R	IC_{50} (nM)
5	DFMP	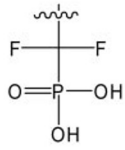	1750
6	Unsaturated IZD	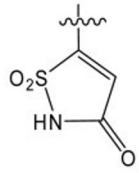	3000
2	Saturated (*R,S*)-IZD	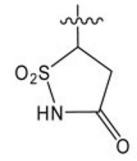	210
7	Saturated (*R*)-IZD	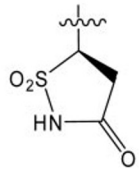	16000
8	Saturated (*S*)-IZD	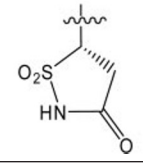	190

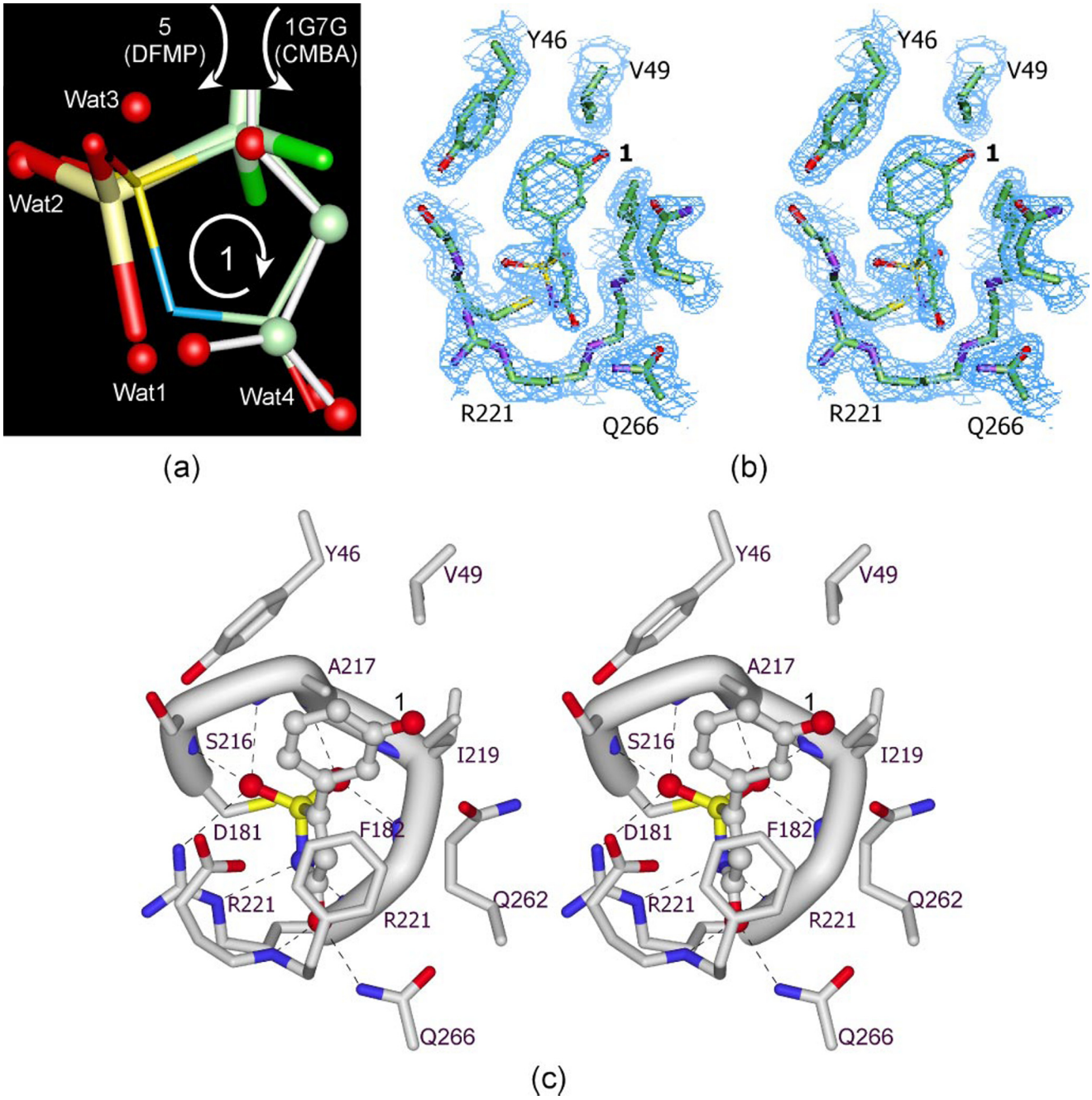

FIGURE 2. **Crystal structure of PTP1B/1.** *a,* superposition of the bound conformations of the phosphonate mimetics of compounds **1**, **5**, and 1G7G. Note the IZD heterocycle of **1** mimics the interactions of DFMP and CMBA, and it displaces four waters. *b,* stereo view of the $2F_o - F_c$ simulated annealed omit map (contoured at 1σ) and atomic model for PTP1B/**1**. The inhibitor was omitted from the model prior to a cycle of simulated annealing and was not used in the calculation of phases. *c,* stereo view of **1** (*ball-and-stick*) bound in the A site. *Dashed lines* indicate 10 potential hydrogen bonds between the inhibitor and residues in the active site.

apoprotein in the $P3_12_1$ space group revealed the presence of three water molecules that bind in the same locations as the phosphonate oxygens of Tyr(P)-containing substrates (25). To confirm that the observed water structure is independent of crystallization conditions and space group, we solved the structures of the apoprotein in two additional space groups, $P2_12_12_1$ (Fig. 3*a*) and C2, as well as the reported $P3_121$. Four tightly bound water molecules (Wat1–4) are observed in each structure, except the C2 structure that does not contain Wat4 (Fig. 3*b*). Three of the waters hydrogen bond to backbone nitrogens of the phosphate-binding loop: Wat1 hydrogen bonds to Arg^{221}, Wat2 to Ile^{219} and Gly^{220}, and Wat3 to Ser^{216} and Ala^{217}. The fourth water hydrogen bonds to the side chain of Gln^{266}. Other waters in the A site are not conserved between the structures and thus probably interact weakly with the protein. The second aryl phosphate-binding site (B site) is also highly solvated: five conserved waters are located near Arg^{254}. The most tightly bound water, based on electron density, is Wat5, which hydrogen bonds directly to the side chain Arg^{254} and appears to organize the surrounding water. Importantly,

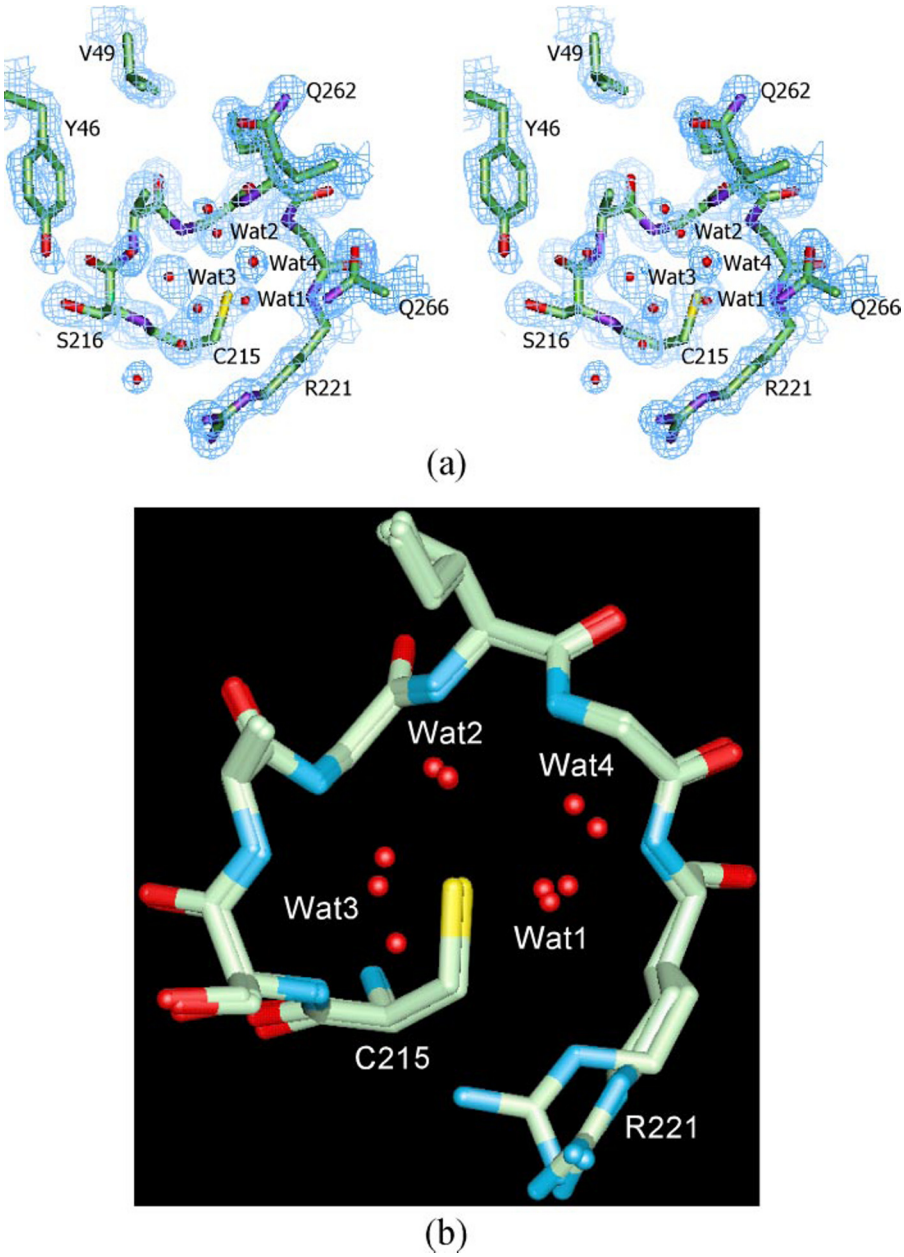

FIGURE 3. **Conserved waters in the A site of apoPTP1B ($P2_12_12_1$).** *a,* stereo view of the atomic model for apoPTP1B and $2F_o - F_c$ electron density map (contoured at 1σ) calculated prior to adding water. *b,* superposition of three apostructures ($P2_12_12_1$, C2, and $P3_121$) reveals the presence of four conserved waters in the A site. Note the position of Wat2 in the three structures is almost identical, and Wat4 is not present in the C2 structure.

the presence of Wat2, Wat3, and most of the conserved B site waters does not appear to be an artifact of the low temperature data collection, because they are also present in the $P2_12_12_1$ apostructure solved at 4 °C. Finally, our trigonal structure is identical to the reported structure, containing a glycerol in the hydrophobic half of the A site and a mixture of opened and closed conformations of the flap (Phe^{180}–Ile^{184}). The disordered conformation of the flap and the presence of glycerol, however, do not appear to influence the water structure associated with the phosphate-binding loop because the waters are also present in our $P2_12_12_1$ and C2 apostructures that only contain the opened conformation of the flap.

A superposition of apoPTP1B ($P2_12_12_1$) and PTP1B in complex with the unsaturated IZD **4** (Table 2; our highest resolution structure) reveals that the IZD-phenyl moiety displaces at least nine waters, more then any other Tyr(P) mimetic (Fig. 4). The sulfone oxygens and nitrogen anion displace Wat1–Wat3; the carbonyl oxygen and phenyl each displace two waters, and the side chain of Arg^{221} which shifts as a result of ligand binding displaces two waters. The three phosphate oxygens of the DFMP moiety of **5** displace Wat1–Wat3 but not Wat4, which shifts by 1.5 Å to accommodate one of the fluorine atoms and remains trapped under the flap where it hydrogen bonds to the fluorine atoms of DFMP, the backbone NH of Phe^{182}, and side chain of Gln^{266}. The CMBA moiety of the PDB entry code 1G7G only displaces Wat1 and Wat4, and the OTCA of 1C83 displaces Wat1–Wat3 but traps Wat4. So far IZD and the recently reported thiadiazolidinone (26) heterocycles are the only phosphonate mimetics that possess a single negative charge and displace all waters in the A site of the closed conformation of the protein.

IZD-Phenol Induces the Closed Conformation of the Protein—To identify conformational changes in the protein induced by IZD-containing inhibitors, we first identified the flexible regions of the protein by superimposing the three apostructures, which were crystallized in different crystal systems ($P3_121$, C2, and $P2_12_12_1$) (Fig. 5*a*). Except for minor shifts at the N and C termini and in solvent-exposed loops, the structures are very similar (r.m.s.d. on C-α atoms is only 0.45 Å). Second, a superposition of PTP1B in complex with four inhibitors crystallized in three crystal systems revealed that all ligands induce very similar conformations of the protein, except for differences in two surface loops (Glu^{115}–Lys^{120} and Lys^{128}–Glu^{132}) and at the N terminus (residues 1–18), where the His_6 affinity tag is attached and β-octyl glucoside binds. Finally, a superposition of the apo- and complexed structures reveals that inhibitors induce two major conformational changes, after excluding the flexible regions identified in the apostructures. The first is the well documented 8 Å shift of the flap (Phe^{180}–Ile^{184}) toward the active site, creating the closed conformation of the protein (Fig. 5*b*) (15). Flap

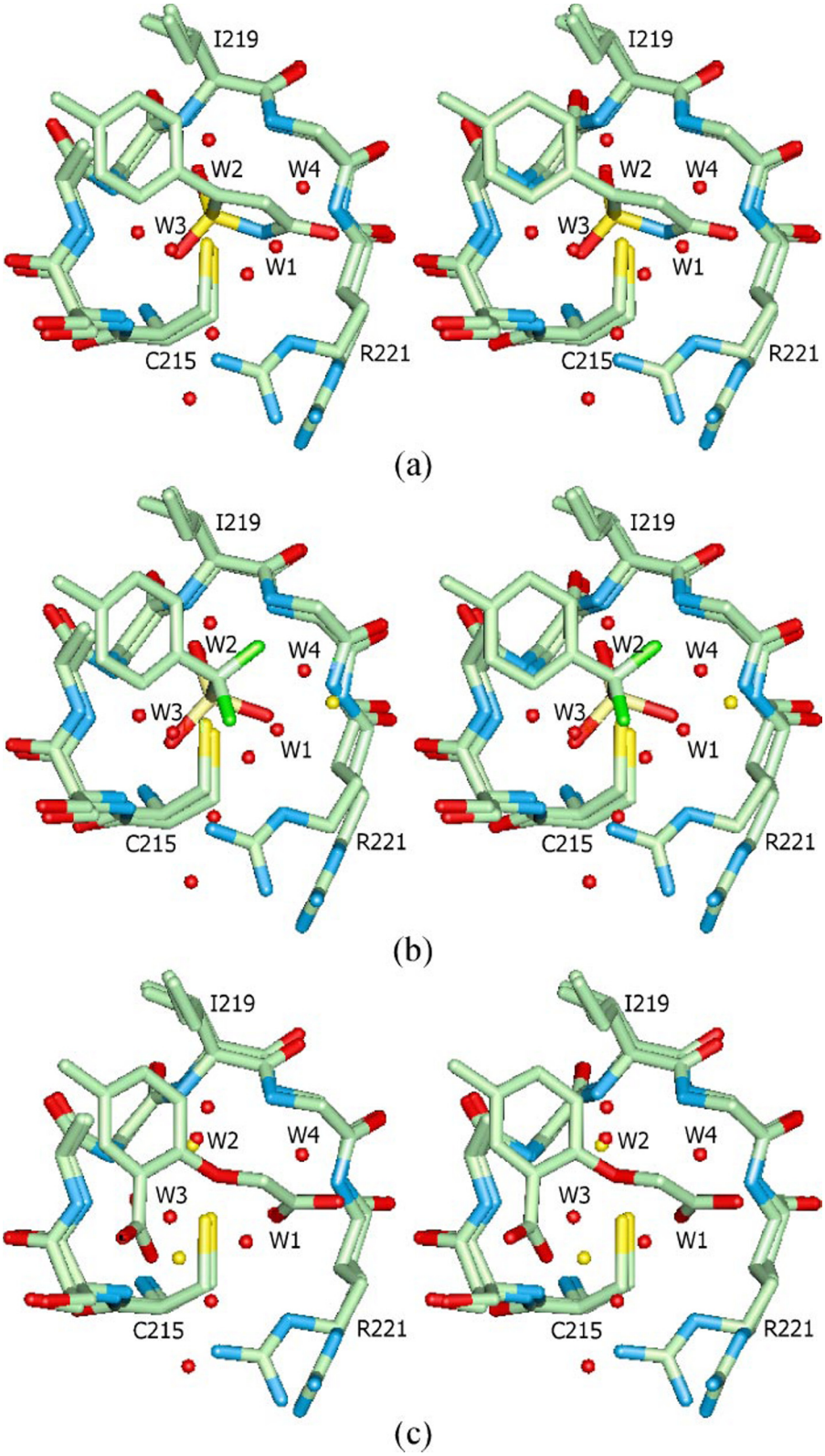

FIGURE 4. **A site waters displaced by phosphotyrosine mimetics.** Superpositions of the orthorhombic apostructure and PTP1B complexed with **4** (*a*), **5** (*b*), and 1G7G (*c*). *Red spheres* represent waters observed in the apostructure, and *yellow spheres* are waters observed in the complexed structures. Note IZD is the only moiety that displaces all waters in the A site. Only the Tyr(P) mimetics of each inhibitor are shown for clarity.

movement is important for catalysis because it brings the general acid Asp[181] into position to protonate the tyrosyl leaving group and positions the flap over the active site where it shields the catalytic machinery from solvent during catalysis. The second conformational change induced by inhibitor binding is a rigid body shift of the C-terminal helix away from the active site, a movement needed to accommodate the closed conformation of the flap. To date, all IZD-containing inhibitors, even the small IZD-phenol **1**, stabilize the closed conformation of the protein through interactions between the hydrophobic half of the IZD-phenyl moiety and side chain of Phe[182] in addition to hydrogen bonds between the carbonyl oxygen of the heterocycle and side chain of Gln[266] and backbone nitrogen of Phe[182].

Saturated IZD-Phenyl Binds Close to Its Conformational Energy Minimum—The crystal structure of PTP1B/**1** reveals that the relative angle between the unsaturated IZD heterocycle and the phenyl ring directly attached to it is 70–75° (Fig. 6*a*). Given that the theoretical optimal angle for the two rings is only 35°, the moiety adopts a high energy conformation when bound to the protein. The energy minimum at 35°, which represents the optimal compromise between maximal *p*-orbital overlap (0°) and minimal steric clash (90°), was determined by calculating the conformational energy of the ring system at various angles from 0 to 180°, using the 6–31G* basis set and the program Spartan (Wavefunction, Inc.). Based on these data, an energy penalty of 1.5–1.8 kcal/mol must be paid to organize the unsaturated heterocycle and phenyl ring into the observed orthogonal orientation. The predicted minimum energy conformation for the saturated IZD-phenyl moiety, however, is very similar to the nearly orthogonal conformation observed in the crystal structure of PTP1B/**2** (Fig. 6*b*). This suggests that saturated IZD analogs should be ~13–19-fold more potent than unsaturated analogs, because both groups have very similar bound conformations, and their heteroatoms interact with the same residues in the A site. The (*S*)-IZD isomer of **2** was determined to be the active compound as it was the only isomer present in the crystal structure even though the

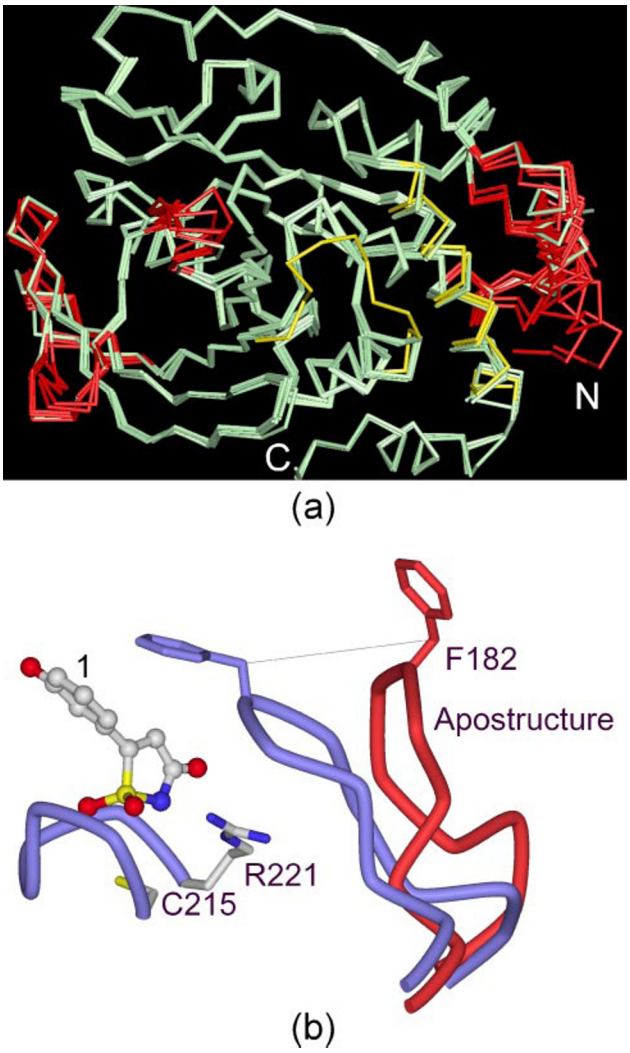

FIGURE 5. **Conformational changes induced by IZD heterocycles.** *a,* superposition of apoPTP1B ($P2_12_12_1$) and five inhibitor complexes crystallized in three different space groups. Except for the N terminus (*N*) and four solvent-exposed loops (*red bonds*), all inhibitors induce similar closed conformations of the protein. *Yellow bonds* indicate regions of the apostructure (flap and C-terminal helix) that differ significantly from the complexed structures. The inhibitors were omitted for clarity. *b,* close-up of the A site showing flap (Thr^{177}–Pro^{188}) movement (8 Å based on the C-β of Phe^{182}) that occurs upon binding compound **1**.

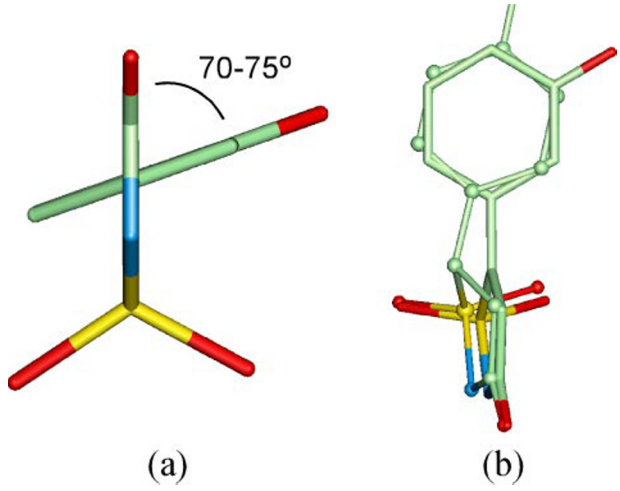

FIGURE 6. **Bound conformations of saturated and unsaturated IZD-phenyl moieties.** *a,* the relative angle between the unsaturated IZD and phenyl rings of **1** is ~70–75°. *b,* superposition of the unsaturated IZD **1** (*stick bonds*) and the saturated (*S*)-IZD-phenyl moiety of **2** (*ball-and-stick*). Note the phenyl ring and heteroatoms of IZD bind in the same position whether or not the heterocycle is reduced.

protein was crystallized in the presence of a diastereoisomeric mixture. The *S* isomer of **2** (compound **8**) was subsequently purified and shown to be 84-fold more active than the *R* isomer **7** (Table 3) (20). The structural data therefore suggests that the saturated (*S*)-IZD **8** is 16-fold more potent than its unsaturated analog **6** because of its lower conformational energy.

Interactions between the Peptide Scaffold of the Inhibitor and the Protein—The IZD heterocycle was incorporated into a peptide to identify key binding interactions outside of the A site that might aid the design of nonpeptidic inhibitors as well as facilitate comparisons between heterocycles and other phosphonate mimetics such as DFMP. One of the first peptides synthesized was the bis-saturated IZD **4**, which has an IC_{50} value of 65 nM, a modest increase compared with **1** given the large increase in molecular weight. The crystal structure of PTP1B/**4** reveals that the inhibitor binds in the A site and extends into the C site, a region previously observed to interact with the distal DFMP moiety of bis-DFMP peptides (18, 27, 28). The distal heterocycle is disordered (the average temperature factor for atoms in the heterocycle is 56 $Å^2$) but appears to interact with the side chain of Lys^{41}, and the aryl ring attached to it is in van der Waals contact with the hydrophobic portion of the side chain of Arg^{47} (Fig. 7*a*). The benzyl group binds over the carboxamide of the inhibitor and does not interact significantly with the protein. This conformation, however, is probably an artifact of crystallization because the benzyl is involved in crystal contacts and its $\chi 1$ angle differs by 90° from that of **3**, which was crystallized in a space group that does not have interfering crystal contacts. The most favorable interactions appear to occur near the A–C site border where the carboxylate of Asp^{48} hydrogen bonds to the carboxamide and α-amino groups, and the backbone nitrogen of Arg^{47} hydrogen bonds to the oxygen of the most distal amide of the inhibitor. Finally, a superposition of PTP1B/**4** and **1** reveals that the bound conformation of the unsaturated IZD-phenyl moiety is not altered by the large peptide scaffold of **4** (Fig. 7*b*). Overall, this analysis implies that **4** is only 21-fold more potent than **1** (Table 2) because the only significant interactions between the inhibitor and the flat, solvent-exposed C site are hydrogen bonds between the peptide scaffold of the inhibitor and the carboxylate of Asp^{48} and backbone NH of Arg^{47}.

As expected, the peptide scaffolds of saturated and unsaturated IZD-containing inhibitors bind very similarly in the C site. A superposition of PTP1B/**3** and **4** reveals that the conformations of the scaffolds only deviate where they differ structurally (Fig. 8*a*) or are influenced by crystal contacts (as mentioned above). In PTP1B/**3**, the carboxamide and α-amino groups hydrogen bond to Asp^{48}; the benzyl binds between the side chains of Arg^{47} and Asp^{48}, and the carbonyl of the benzamide cap hydrogen bonds to the backbone nitrogen of Arg^{47}. The only notable interaction not previously observed in PTP1B/**4** is a π-stacking interaction between the aryl ring of the benzamide cap and the guanidinium side chain of Arg^{47}; this interaction,

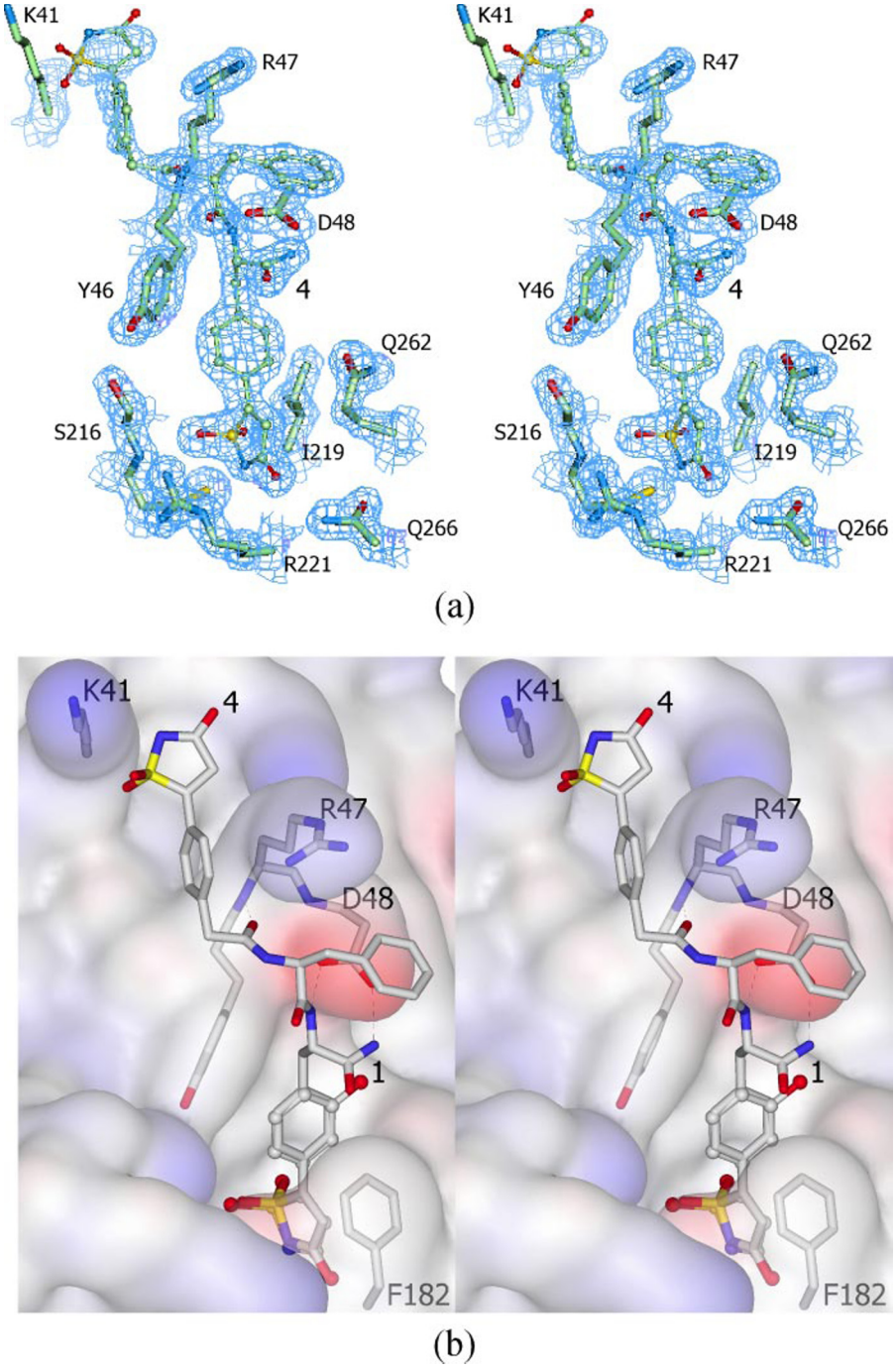

FIGURE 7. **Crystal structure of PTP1B/4.** *a,* stereo view of the $2F_o - F_c$ simulated annealed omit map (contoured at 1σ) and atomic model for PTP1B/**4**. The inhibitor was omitted from the model prior to a cycle of simulated annealing and was not used in the calculation of phases. Note the distal IZD-phenyl moiety is the least well defined region of the inhibitor. *b,* superposition of PTP1B/**4** (surface and *stick bonds*) and **1** (*ball-and-stick*) reveals that the peptide scaffold of **4** does not alter the bound conformation of the IZD-phenyl moiety. *Dashed lines* indicate hydrogen bonds between **4** and backbone nitrogen of Arg[47] and side chain of Asp[48].

however, is probably fairly weak because the side chain of Arg[47] is solvent-exposed. These results highlight the importance of interacting with the C site through peptidic hydrogen bonds and explain why **3** and its truncated analog **2** are equipotent (Table 2).

Finally, the crystal structures of PTP1B in complex with the saturated IZD **2** and its DFMP analog **5** provide a direct comparison between the two phosphonate mimetics. A superposition of the structures reveals that the peptide scaffolds bind very similarly (Fig. 8*c*). This suggests that **8** (the *S* isomer of **2**) is 9 times more potent than **5** (Table 3) because the saturated IZD heterocycle is a more potent phosphonate mimetic for PTP1B. The structure of PTP1B/**2** also indicates that the peptide scaffold of the inhibitor can be further truncated without a significant decrease in potency because the C site benzyl group, which binds between Arg[47] and Asp[48], is fairly disordered (Fig. 8*b*).

DISCUSSION

PTP1B is a particularly challenging drug discovery target because its active site is highly charged, fairly flat, and solvent-exposed. Although this surface is ideal for binding large polar substrates like the insulin receptor, which possesses at least three phosphotyrosines, it significantly complicates the design of potent small molecule inhibitors. The requirement to complement a charged surface coupled with a lack of binding determinants outside of the primary phosphate-binding pocket (A site) has resulted in the design of fairly large inhibitors that contain highly charged phosphonate mimetics (Fig. 1). Our attempt to improve the potency and physicochemical properties of PTP1B inhibitors has recently led to the discovery of a novel five-membered IZD heterocycle (20). When substituted with a phenyl ring, IZD is one of the most potent PTP1B phosphotyrosine mimetics reported to date. Compared with the *para*-difluorophosphonomethylphenyl Tyr(P) mimetic, which has a K_i value of 2.5 mM (29), the unsaturated IZD-phenol **1** is a potent inhibitor for its size (IC_{50} = 1.35 μM) (Table 2).

The high potency of the IZD heterocycle can be attributed to a combination of several factors. First, IZD binds at the center of the phosphate-binding loop where it interacts with the positive end of the helix dipole of α4 (Arg[221]–Arg[238]) and participates in an extensive network of hydrogen bonds (Fig. 2*c*). In fact, every hydrogen bond donor in the phosphate-binding loop is less than 3.3 Å from one of the four heteroatoms of IZD. This high degree of charge complementarity increases potency by reducing the destabilizing effect of dehydration of the polar phos-

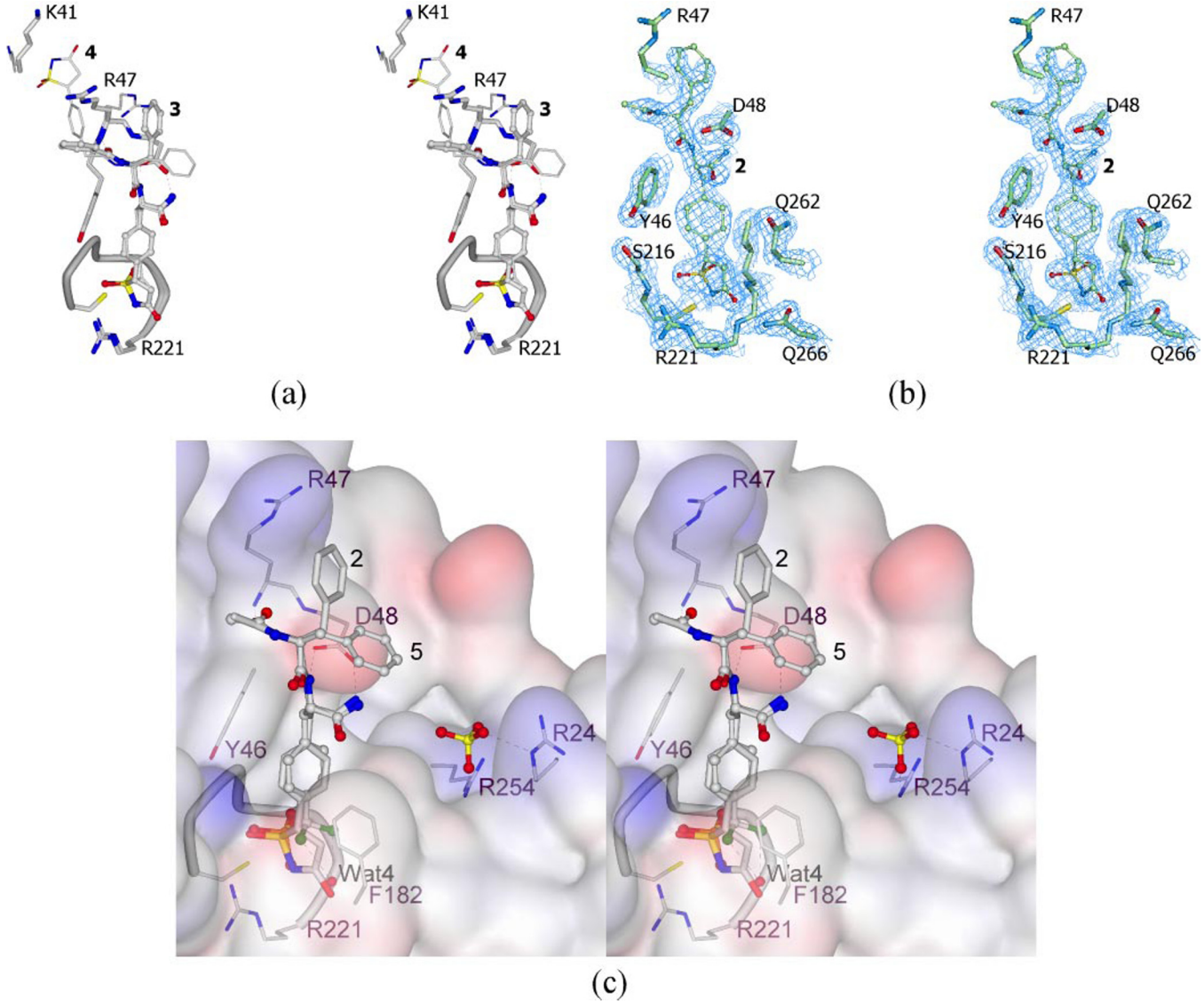

FIGURE 8. *a,* superposition of PTP1B/**3** (*ball-and-stick* and *thick bonds*) and **4** (*thin bonds*) reveals that the bound conformation of the peptide scaffold is very similar whether or not the heterocycle is saturated or unsaturated. The only differences are due to crystal contacts (not shown) in the PTP1B/**4** (compare benzyl substituents) and structural differences between the inhibitors. *b,* stereo view of the $2F_o - F_c$ simulated annealed omit map (contoured at 1σ) and atomic model for PTP1B/**2**. The inhibitor was omitted from the model prior to a cycle of simulated annealing and was not used in the calculation of phases. The entire inhibitor is very well defined except for the benzyl group, which binds between Arg^{47} and Asp^{48}. Note only the (*S*)-IZD isomer of **2** crystallized in complex with PTP1B, even though a diastereoisomeric mixture was present during crystallization. *c,* superposition of PTP1B/**2** (surface and *thick* and *thin bonds*) and **5** (*ball-and-stick*) reveals that IZD and DFMP project the peptide scaffold in exactly the same position in the C site. Note Wat4 hydrogen bonds to DFMP, and a sulfate ion in the B site hydrogen bonds to Arg^{24} and Arg^{254} in PTP1B/**5**; the protein of the latter was omitted for clarity.

phate-binding loop upon ligand binding (30). Second, the IZD-phenyl moiety displaces all tightly bound waters in the A site (Fig. 4*c*). Because this region is highly solvated and the entropic gain from displacing a single structural water molecule has been estimated to be as high as 2 kcal/mol (31), we believe the high binding affinity of IZD is in part due to the displacement of at least three tightly bound waters in the A site. PTP1B in complex with other phosphonate mimetics, such as OTCA, CMBA, oxalylaminobenzoic acid, and DFMP, retains one or two waters in its A site. For example, the two fluorines of DFMP hydrogen bond to Wat4 and trap it under the flap of the protein (Phe^{180}–Ile^{184}), whereas the carbonyl of the heterocycle displaces Wat4 and hydrogen bonds directly to the backbone nitrogen of Phe^{182} and side chain of Gln^{266}. Third, the heterocycle, IR kinase activation segment, and most phosphonate mimetics all induce the same closed conformation of the protein (Fig. 5*b*). Although this is not a prerequisite for high affinity binding, stabilizing the closed conformation increases the interaction surface area between the protein and inhibitor and potentially reduces the rate of dissociation of the complex. But more importantly, this observation indicates that the conformationally constrained IZD heterocycle mimics the interactions of the substrate and other more flexible phosphonate mimetics. The preorganized heterocycle should therefore have a lower entropy penalty associated with binding. Finally, the bound conformation of the saturated (*S*)-IZD-phenyl moiety corresponds to its conformational energy minimum (Fig. 6*b*). We believe all of these characteristics contribute to the high potency of IZD heterocycles and explain why (*S*)-IZD **8** is 9-fold more potent than its DFMP analog **5** (Table 3).

The IZD heterocycle was also designed to address the poor membrane permeability of reported PTP1B inhibitors. We postulated that the heterocycle would have improved cell permeability compared with the hard charged phosphonate and carboxylate-containing compounds because it possesses a single delocalized charge. Furthermore, analogous acyclic acylsulfonamides are known cell-permeable isosteres for carboxylic acids (32). Although IZD-containing peptides lacked cellular activity because of poor permeability, we have recently reported the design of nonpeptidic IZD-containing inhibitors that have cellular activity in an IR phosphorylation assay (21). The heterocycle therefore provides the possibility of designing potent inhibitors with improved cell permeability.

REFERENCES

1. Frangioni, J. V., Beahm, P. H., Shifrin, V., Jost, C. A., and Neel, B. G. (1992) *Cell* **68,** 545–560
2. Saltiel, A. R., and Kahn, R. (2001) *Nature* **414,** 799–806
3. Elchebly, M., Payette, P., Michaliszyn, E., Cromlish, W., Collins, S., Loy, A. L., Normandin, D., Cheng, A., Himms-Hagen, J., Chan, C.-C., Ramachandran, C., Gresser, M. J., Tremblay, M. L., and Kennedy, B. P. (1999) *Science* **283,** 1544–1548
4. Klaman, L. D., Boss, O., Peroni, O. D., Kim, J. K., Martino, J. L., Zabolotny, J. M., Moghal, N., Lubkin, M., Kim, Y.-B., Sharpe, A. H., Stricker-Krongrad, A., Shulman, G. I., Neel, B. G., and Kahn, B. B. (2000) *Mol. Cell. Biol.* **20,** 5479–5489
5. Zinker, B. A., Rondinone, C. M., Trevillyan, J. M., Gum, R. J., Clampit, J. E., Waring, J. F., Xie, N., Wilcox, D., Jacobson, P., Frost, L., Kroeger, P. E., Reilly, R. M., Koterski, S., Opgenorth, T. J., Ulrich, R. G., Crosby, S., Butler, M., Murray, S. F., McKay, R. A., Bhanot, S., Monia, B. P., and Jirousek, M. R. (2002) *Proc. Natl. Acad. Sci. U. S. A.* **99,** 11357–11362
6. Barford, D., Flint, A. J., and Tonks, N. K. (1994) *Science* **263,** 1397–1404
7. Johnson, T. O., Ermolieff, J., and Jirousek, M. R. (2002) *Nat. Rev. Drug Discovery* **1,** 696–709
8. Blaskovich, M. A., and Kim, H.-O. (2002) *Expert Opin. Ther. Pat.* **12,** 871–905
9. Liu, G. (2003) *Curr. Med. Chem.* **10,** 1407–1421
10. Taylor, S. D., and Hill, B. (2004) *Exp. Opin. Investig. Drugs* **13,** 199–214
11. Pei, Z., Liu, G., Lubben, T. H., and Szczepankiewicz, B. G. (2004) *Curr. Pharm. Des.* **10,** 3481–3504
12. Costantino, L., and Barlocco, D. (2004) *Curr. Med. Chem.* **11,** 2725–2747
13. Bialy, L., and Waldmann, H. (2005) *Angew. Chem. Int. Ed.* **44,** 3814–3839
14. Salmeen, A., Andersen, J. N., Myers, M. P., Tonks, N. K., and Barford, D. (2000) *Mol. Cell* **6,** 1401–1412
15. Jia, Z., Barford, D., Flint, A. J., and Tonks, N. K. (1995) *Science* **268,** 1754–1758
16. Andersen, J. N., Mortensen, O. H., Peters, G. H., Drake, P. G., Iversen, L. F., Olsen, O. H., Jansen, P. G., Andersen, H. S., Tonks, N. K., and Møller, N. P. H. (2001) *Mol. Cell. Biol.* **21,** 7117–7136
17. Puius, Y. A., Zhao, Y., Sullivan, M., Lawrence, D. S., Almo, S., and Zhang, Z.-Y. (1997) *Prot. Natl. Acad. Sci. U. S. A.* **94,** 13420–13425
18. Jia, Z., Ye, Q., Dinaut, A. N., Wang, Q., Waddleton, D., Payette, P., Ramachandran, C., Kennedy, B., Hum, G., and Taylor, S. D. (2001) *J. Med. Chem.* **44,** 4584–4594
19. Burke, T. R., Jr., and Lee, K. (2003) *Acc. Chem. Res.* **36,** 426–433
20. Combs, A. P., Yue, E. W., Bower, M., Ala, P. J., Wayland, B., Douty, B., Takvorian, A., Polam, P., Wasserman, Z., Zhu, W., Crawley, M., Pruitt, J., Sparks, R., Glass, B., Modi, D., McLaughlin, E., Bostrom, L., Li, M., Galya, L., Blom, K., Hillman, M., Gonneville, L., Reid, B., Wei, M., Becker-Pasha, M., Klabe, R., Huber, R., Li, Y., Hollis, G., Burn, T. C., Wynn, R., Liu, P., and Metcalf, B. (2005) *J. Med. Chem.* **48,** 6544–6548
21. Combs, A. P., Zhu, W., Crawley, M. L., Glass, B., Polam, P., Sparks, R. B., Modi, D., Takvorian, A., McLaughlin, E., Yue, E. W., Wasserman, Z., Bower, M., Wei, M., Rupar, M., Ala, P. J., Reid, B. M., Ellis, D., Gonneville, L., Emm, T., Taylor, N., Yeleswaram, S., Li, Y., Wynn, R., Burn, T. C., Hollis, G., Liu, P. C. C., and Metcalf, B. (2006) *J. Med. Chem.* **49,** 3774–37789
22. Barford, D., Keller, J. C., Flint, A. J., and Tonks, N. K. (1994) *J. Mol. Biol.* **239,** 726–730
23. Szczepankiewicz, B. G., Liu, G., Hajduk, P. J., Abad-Zapatero, C., Pei, Z., Xin, Z., Lubben, T. H., Trevillyan, J. M., Stashko, M. A., Ballaron, S. J., Liang, H., Huang, F., Hutchins, C. W., Fesik, S. W., and Jirousek, M. R. (2003) *J. Am. Chem. Soc.* **125,** 4087–4096
24. Berman, H. M., Westbrook, J., Feng, Z., Gilliland, G., Bhat, T. N., Weissig, H., Shindyalov, I. N., and Bourne, P. E. (2000) *Nucleic Acids Res.* **28,** 235–242
25. Pedersen, A. K., Peters, G. H., Møller, K. B., Iversen, L. F., and Kastrup, J. S. (2004) *Acta Crystallogr. Sect. D Biol. Crystallogr.* **60,** 1527–1534
26. Black, E., Breed, J., Breeze, A. L., Embrey, K., Garcia, R., Gero, T. W., Godfrey, L., Kenny, P. W., Morley, A. D., Minshull, C. A., Pannifer, A. D., Read, J., Rees, A., Russell, D. J., Toader, D., and Tucker, J. (2005) *Bioorg. Med. Chem. Lett.* **15,** 2503–2507
27. Asante-Appiah, E., Patel, S., Dufresne, C., Roy, P., Wang, Q., Patel, V., Friesen, R. W., Ramachandran, C., Becker, J. W., Leblanc, Y., Kennedy, B. P., and Scapin, G. (2002) *Biochemistry* **41,** 9043–9051
28. Sun, J.-P., Fedorov, A. A., Lee, S.-Y., Guo, X.-L., Shen, K., Lawrence, D. S., Almo, S. C., and Zhang, Z.-Y. (2003) *J. Biol. Chem.* **278,** 12406–12414
29. Yao, Z.-J., Ye, B., Wu, X.-W., Wang, S., Wu, L., Zhang, Z.-Y., and Burke, T. R., Jr. (1998) *Bioorg. Med. Chem.* **6,** 1799–1810
30. Loladze, V. V., Ermolenko, D. N., and Makhatadze, G. I. (2002) (2002) *J. Mol. Biol.* **320,** 343–357
31. Dunitz, J. D. (1994) *Science* **264,** 670
32. Uehling, D. E., Donaldson, K. H., Deaton, D. N., Hyman, C. E., Sugg, E. E., Barrett, D. G., Hughes, R. G., Reitter, B., Adkison, K. K., Lancaster, M. E., Lee, F., Hart, R., Paulik, M. A., Sherman, B. W., True, T., and Cowan, C. (2002) *J. Med. Chem.* **45,** 567–583